ACCEPTED MANUSCRIPT

Local combustion regime identification using machine learning

Riccardo Malpica Galassi[a], Pietro Paolo Ciottoli[a], Mauro Valorani[a], Hong G. Im[b]

[a]Mechanical and Aerospace Engineering Department, Sapienza University of Rome, Via Eudossiana, 18, Rome 00184, Italy;
[b]Clean Combustion Research Center, King Abdullah University of Science and Technology, Thuwal, 23955-6900, Saudi Arabia.

ARTICLE HISTORY
Compiled March 15, 2022

ABSTRACT
A new combustion regime identification methodology using the neural networks as supervised classifiers is proposed and validated. As a first proof of concept, a binary classifier is trained with labeled thermochemical states obtained as solutions of prototypical one-dimensional models representing premixed and nonpremixed regimes. The trained classifier is then used to associate the regime to any given thermochemical state originating from a multi-dimensional reacting flow simulation that shares similar operating conditions with the training problems. The classification requires local information only, i.e., no gradients are required, and operates on reduced-dimension thermochemical states, in order to cope with experimental data as well. The validity of the approach is assessed by employing a two-dimensional laminar edge flame data as a canonical configuration exhibiting multi-regime combustion behavior. The method is readily extendable to additional classes to identify criticality phenomena, such as local extinction and re-ignition. It is anticipated that the proposed classifier tool will be useful in the development of turbulent multi-regime combustion closure models in large scale simulations.

KEYWORDS
Gradient-free regime classification; neural networks; multi-regime reacting flows; tribrachial flames;

1. Introduction

Reacting flows of practical interest are characterized by strong interactions between turbulence, mixing, and chemical reactions, over a wide dynamic range of space and time scales. The unsteady interplay between chemistry and transport phenomena, such as diffusion and advection, is described by partial differential equations. Combustion systems are prone to complexity issues arising from both the dimensionality of the problem, due to a large number of chemical species involved, especially in hydrocarbons combustion, and the stiffness originating from the presence of very different space and timescales. This complexity translates into difficulties in formulating affordable predictive models and is further exacerbated by the general direction in which combustion systems are evolving because of the increasingly stringent requirements on efficiency and emissions, e.g., higher pressures, lower temperatures, and higher levels of dilution.

CONTACT Riccardo Malpica Galassi. Email: riccardo.malpicagalassi@uniroma1.it

Despite the continual growth in size, speed, and availability of large computers, direct numerical simulations (DNS) of all the scales involved in turbulent flows coupled with detailed chemistry, eventually capable of replacing laboratory experiments of real-world combustion systems, will remain unfeasible in the foreseeable future. Even if it is possible, such large scale simulation data do not necessarily provide clear physical insights. Therefore, the efforts into the simplification of the mathematical description of complex physical and chemical processes are necessary. The goal is to develop affordable predictive models which, under specific assumptions, can provide the essential underlying mechanisms that are responsible for the physical problems of interest, such as burning rates, pollutant formation, or criticality phenomena like ignition and extinction.

The premixed versus nonpremixed combustion regimes has been one of the most basic classifications to build the mathematical modeling framework in describing the distinct combustion characteristics. The premixed combustion has both reactants mixed at molecular level, hence the combustion process becomes kinetically controlled, while naturally in balance with reactant transport. On the other hand, the nonpremixed combustion process is dominated by the transport which brings the separated reactants into the reaction zone. As such, distinct reaction closure models are employed in turbulent reacting flow simulations in order to represent the crucial behavior of different combustion regimes.

However, such a combustion regime identification is not always straightforward in real applications. Many modern combustion systems are purposely designed to operate in the *partially* premixed mode to achieve higher efficiencies and lower emissions. Examples are present in gas turbines, aircraft combustors, direct-injection engines, and industrial combustion systems. According to Masri [1], partial premixing refers to the existence in the fresh mixture of composition inhomogeneities, which evolve due to mixing so that both diffusion-like reaction zones and premixed propagating layers may coexist. A canonical example is the lifted flame edge, which propagates into a mixture with stratification in the lateral direction [2]. The stabilization of the flame depends on the tribrachial structures characterized by a lean premixed branch, a rich premixed branch, and a trailing diffusion flame that forms behind the premixed flame front because of the mixing of the excess oxidizer and fuel [1, 3, 4].

Laminar triple flames have commonly been employed as test-beds for assessing the validity of combustion models aimed at dealing with multi-mode configurations. Van Oijen and de Goey [5] tested the flamelet generated manifold (FGM) technique against a detailed chemistry approach on a triple flame. Domingo et al. [6, 7] proposed a subgrid combustion closure model in the large eddy simulation (LES) context for partially premixed systems, with the closure building upon the association of the locally resolved field to either a premixed or a nonpremixed model. The technique is tested on a turbulent lifted flame. Knudsen and Pitsch [8, 9] developed a multi-mode flamelet model, capable to locally select whether tabulated premixed or tabulated nonpremixed chemistry should be referenced in the presumed probability density function (PDF) of large eddy simulations (LES). The model was tested in a laminar triple flame configuration.

Most of these approaches for hybrid combustion models [6, 8, 9] need a rational criterion to determine whether the local reacting flow belongs to the premixed or nonpremixed combustion mode. For this purpose, the flame index, introduced by Yamashita et al. [10] and then revised in a normalized version by Domingo et al. [7], is the most traditional combustion regime identifier. It builds upon the examination of the fuel and oxidizer gradients. Their alignment/misalignment, determined by the sign and magnitude of the product of the two gradient vectors, serves as the metric

for relative dominance of premixed or nonpremixed combustion regime. Fiorina et al. [11] proposed an improved flame index accounting for finite rate chemistry effects in strained diffusion flames.

Even though the flame index proved to be a reliable indicator of combustion regimes, it requires knowledge of non-local information, i.e., spatial gradients. This raises difficulties in experiments [4], since simultaneous 3D gradients of fuel and oxidizer fields are needed. Rosenberg et al. [12] proposed a method to measure the flame index based on 2D images of fluorescent markers, which however can be misleading if the scalar field has pronounced 3-dimensional features. A gradient-free, hence local, sensor of combustion regimes would be desirable, as pointed out by Hartl et al. [13].

From a mathematical standpoint, the two regimes differ in the way the advection, diffusion, and chemical source terms are balanced in the conservation equations. Hence, the dynamics of the system is differently constrained to specific regions of the chemical composition space, leading to distinct low-dimensional manifolds characterizing the essential slow dynamics. The existence of manifolds in homogeneous reacting systems is well understood, and many available model reduction techniques are based on the constraints on the thermochemical states to a low-dimensional region of the composition space. Examples are the intrinsic low-dimensional manifold (ILDM) technique [14] and the computational singular perturbation (CSP) [15]. A manifold in the chemical composition space develops because the fast chemical processes equilibrate, constraining the dynamics to evolve on a lower-dimensional surface exhibiting the important slow dynamical behavior.

More recent studies [16–18] investigated slow manifolds in non-homogeneous reaction systems involving transport in addition to chemical reactions. Goussis et al. [19] incorporated the effects of diffusion on the chemically slow manifold, analyzing the cases where transport acts as a perturbation driving the system off the chemical manifold, with the fast chemical processes rapidly relaxing the system back onto it. It was shown that a modified slow manifold can be determined by the exhausted fast time scales related to both chemical reactions and diffusion. Najm et al. [20] examined the effective low-dimensional structure of the chemical manifold in a methane–air edge flame. Mengers and Powers [21] applied the concept of slow manifolds to chemical systems with diffusion, using the Galerkin method to reduce the governing PDEs into a system of ODEs, and analyzing the shift in the time-scale spectrum due to the diffusion operator at different resolved wavelengths.

Bykov and Maas [22] proposed the Reaction–Diffusion Manifold (REDIM) as an extension of ILDM which approximates low-dimensional attracting manifolds of PDEs. In flamelet-generated manifolds (FGM), flamelet equations are solved to yield one-dimensional [23] or multi-dimensional manifolds [5] in chemical composition space spanned by suitable variables, e.g., mixture fraction and progress variable. In the multidimensional flamelet-generated mainfold (MFM) method [24], specifically developed to address the existence of different combustion modes, multidimensional flamelet governing equations are derived by projecting the full set of unsteady mass and species conservation equations onto a five-dimensional subspace, involving mixture fraction, progress variable and three scalar dissipation rates. Similarly, the principal component analysis (PCA) proposed by Sutherland and Parente [25] aims at finding an optimal basis for identifying low-dimensional structures based on the training data to efficiently describe the thermochemical state evolution. Echekki and Mirgolbabaei [26] employed PCA on a database generated with simplified problems to reduce the composition space, and then transport the principal components in a turbulent flame problem.

All these methods have a common goal to seek a dimensional reduction in the com-

position space where the system is actually evolving, with the aim of reducing the computational cost by developing lower-dimensional models. A basic underlying hypothesis in these approaches is that any physical behavior of interest can be described by a minimal set of appropriate projection bases. The bases may be heuristically determined by physical variables such as mixture fraction and/or progress variables, or by mathematical operations such as eigenvectors or principal components.

In general, the local thermochemical states reached by a transport-reaction problem are different segregated regions of the chemical composition space depending on how and to what extent the thermochemical system is perturbed by transport. A similar assumption is made by Hartl et al. [13] in that the local thermochemical state depends on the combustion regime and can be considered a "footprint". They proposed a method of gradient-free regime identification (GFRI) that relies on a combination of flame markers, namely mixture fraction, chemical explosive mode analysis, and heat release rate. Wu and Ihme [27] defined a regime marker based on drift terms which describe how well a given manifold-based combustion model can represent the local flow and flame conditions. Zirwes et al. [28] employed different existing regime markers, namely the gradient-based flame index, the GFRI and the drift terms, to distinguish between premixed and nonpremixed local regimes in a partially premixed turbulent Sydney/Sandia flame.

We hereby employ Machine Learning to exploit the intrinsic low-rank features of combustion regimes. More specifically, the conjectured segregation in the composition space of the thermochemical states originating from different combustion regimes should enable a properly trained classifier to identify a state belonging to either the premixed or the nonpremixed mode, without additional spatial information originating from gradients.

A classifier is an application of supervised machine learning, in which the algorithm is presented with labelled datasets. The best model for the given labeled data is then found via optimization [29]. This model is then used for classification of new data. In other words, during a training phase the classifier learns the manifolds generated by different prototypical problems. This training phase yields a model which is capable of assigning a probability of belonging to a specific manifold, or class, to a given new thermochemical state, whose association with a combustion regime is not known a-priori, because, say, it is obtained as a solution of a complex, partially mixed, reacting flow in multidimensional CFD simulations.

Classifiers in numerical combustion have been employed by Grogan and Ihme [30] to discriminate between regular combustion and irregular ignition regimes in detonations, analyzing experimental data from disparate sources. They concluded the analysis stating that the correct classification of the combustion process under study is low dimensional, after assessing the relative importance of the features, i.e., parameters employed to label the data. On the other hand, unsupervised algorithms discover patterns in the data without given labels and generate clusters. In this context, D'Alessio and coworkers [31] classified the composition space via classifiers defined *a priori*. They partition the chemical composition space in a prescribed number of clusters with similar composition using k-Means and Local Principal Component Analysis (LPCA). Each cluster then undergoes a kinetic mechanism reduction, to enable adaptive chemistry in CFD simulations.

In this work, we propose to train a neural-network-based classifier with labeled thermochemical states originating from steady 1D laminar premixed and nonpremixed models, solved by assigning proper boundary conditions. The trained classifier is then employed to classify the local states in a numerical simulation of a laminar edge flame

with consistent boundary conditions. A reliable and non-expensive classification of combustion regimes might (i) shed light on optimal low-rank subspaces in chemical composition space, (ii) support multi-regime combustion closures in LES, and (iii) facilitate classification in experiments without the need of spatial information. In consideration of the latter, the classifier will be trained and tested using the subset of species from the full thermochemical state representing the Raman/Rayleigh measurable species, as done in [13].

This application of machine learning to combustion regime identification is far from being comprehensive, but rather serves as a proof of concept. For example, unsteady effects are not considered, since the inspected edge flame is steady and its reactants are cold. As a consequence, auto-ignition and extinction dynamics are not present and left aside in the training process. However, the conceptual framework is general, and a proper training on unsteady homogeneous reactors and/or unstable branches of the S-shape curve should allow the classifier to be appropriately trained for such combustion modes as applicable. The extension to other regimes, such as auto-ignition, does not pose particular challenges, except that the training dataset should be built including samples generated with the appropriate archetypal models. As such, the present approach can be extended to multi-class identification without major modifications, as long as archetypal models for training are available and well-characterized.

The latter caveat deserves a further discussion: our conjectured segregation in the composition space of the thermochemical states originating from different combustion regimes depends on the definition of the combustion regime itself. We assume this definition as being implicit in the existence of an archetypal model. As long as different models produce different realizations of thermochemical states, such states, or states close to those embeddings, can be identified by a properly trained classifier. However, the ability of any archetypal models to accurately describe the physics of distinct classes of reacting flows is beyond the scope of the present study. Ultimately, the aim of this work is to demonstrate that a properly trained classifier is able to identify the segregation between premixed and nonpremixed embeddings in the thermochemical composition space based on state functions alone.

To this end, we purposely limit the number of classes to two, following the numerous studies [6–9] on binary regime identification and consequent two-model tabulation closure strategies, which are unambiguous and consolidated. Lastly, the actual application to combustion closure would require training and testing on filtered composition and temperature data, which is not addressed in this work.

The paper is organized as follows: neural networks for classification problems are presented in section 2, the training and testing of the classifier, as well as the numerical setup of the edge flame test case, are presented in section 3. Finally, the classification outcomes on the edge flame are discussed and compared with the consolidated gradient-based flame index in section 4.

2. Method

Supervised machine learning algorithms are built to exploit the intrinsic low-rank features of labeled data sets [29, 32]. The goal is to build a model for the given labeled data, which is then employed to classify new data. The model-building phase is essentially the extraction of a typically nonlinear function that characterizes the boundary between data belonging to different classes. The higher the dimension of the full space, the more complicated the data embeddings, the more difficult it would be to

extract a meaningful and general boundary, or hypersurface, that assures an optimal separation between the distributions of points.

Many classification algorithms are available, such as k-nearest Neighbors (kNN), which assigns a label to new data based on the k nearest neighbours labels; the regression tree, which splits the data producing branches of the tree structure; Support Vector Machine (SVM), which projects the data to seek an hyperplane to split them; and Naive Bayes, which estimates the label of new data based on the prior probability distributions of the labeled data. Details on supervised methods can be found in [29]. These algorithms are being replaced by Neural Networks [32].

A Neural Network (NN) is a multi-layer mapping between an input layer $\boldsymbol{x}$ and an output layer $\boldsymbol{y}$. A NN is a mapping of the form:

$$\boldsymbol{y} = \boldsymbol{A}_M \boldsymbol{A}_{M-1} ... \boldsymbol{A}_2 \boldsymbol{A}_1 \boldsymbol{x} \tag{1}$$

where the matrices $\boldsymbol{A}_j$ contain the coefficients that map each variable from one layer to the next. A non-linear NN employs non-linear activation functions to connect the layers:

$$\boldsymbol{y} = f_M(\boldsymbol{A}_M, f_{M-1}(\boldsymbol{A}_{M-1}, ..., f_2(\boldsymbol{A}_2, f_1(\boldsymbol{A}_1, \boldsymbol{x})))). \tag{2}$$

Training a NN means finding the entries of the connectivity matrices $\boldsymbol{A}_j$ through optimization, knowing $\boldsymbol{x}$, i.e., the input, and $\boldsymbol{y}$, i.e., the associated output, such that the mapping error between $\boldsymbol{y}$ and the true (or target) output is minimized. Neural Networks in classification tasks are trained to map new data $\boldsymbol{x}^*$ into their correct label, hence the output is a label, or class, and the training is devoted to minimize the error between the true class and the predicted class. In the case of the present binary classification, the dimensionality N of the input layer is the chemical composition space dimension N_s plus temperature, while the output layer is a sole perceptron $\boldsymbol{y} = \{premixed, nonpremixed\}$, as shown in Fig. 1, in such a way that:

$$\boldsymbol{y} = \begin{bmatrix} 1 \\ 0 \end{bmatrix} = \{\text{premixed}\} \qquad \boldsymbol{y} = \begin{bmatrix} 0 \\ 1 \end{bmatrix} = \{\text{nonpremixed}\} \tag{3}$$

It would be natural to interpret the output $\boldsymbol{y}$ in probabilistic terms, so that the two entries y_i of $\boldsymbol{y}$ are the posterior probabilities $P(\text{class}_i \,|\, \boldsymbol{x}^*)$, i.e., the probability that the correct label of $\boldsymbol{x}^*$ is class_i. Hence, the quantity y_i can be given the meaning of confidence of the classification result [33]. Some classifier models are naturally based on probability density estimates, such as Naive Bayes and logistic regression. Feed forward neural networks with non-linear activation functions, such as sigmoids, can easily be given continuous outcomes on the $[0, 1]$ interval, such that they approximate the posterior probabilities for well trained and sufficiently large networks [34]. The capability of a neural network to provide outputs which estimate *a posteriori* probabilities has been proved in many works [35–41], particularly in the context of classifiers. This is especially true when the loss function employed to calibrate the network is the cross-entropy function, which measures the difference between the true and the predicted probability distributions. A hard classification can be done employing decision rules, e.g. the predicted class among the two is the one having the highest probability.

The number of layers and the activation functions are tunable parameters of the algorithm. For instance, a deeper network will be able to fit more complex patterns but will be more prone to overfitting. To the extent of this work, we rely on the Neural

Network classifier built in Wolfram Mathematica, which offers state-of-the-art capabilities for the construction, training and deployment of neural network machine learning systems. The Mathematica classifier makes the choices of the algorithm parameters automatically through a procedure consisting of experiments done on data subsets.

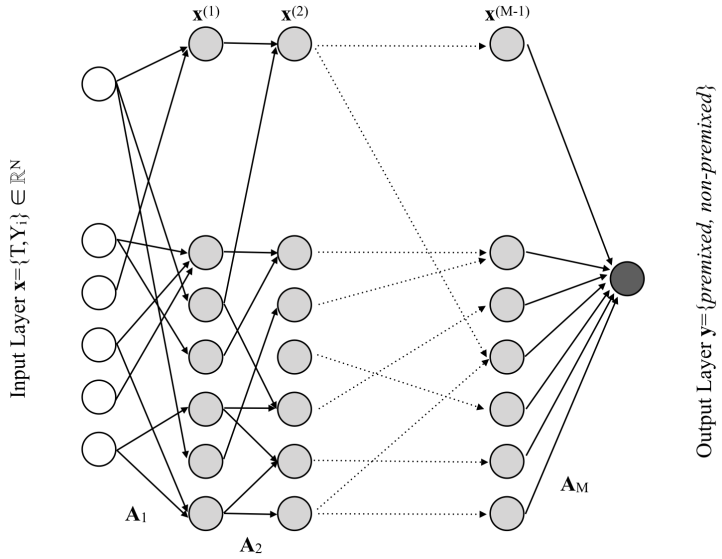

Figure 1.: Sketch of a multi-layer neural network with M levels, that maps an input $\boldsymbol{x} \in \mathbb{R}^N$ to a single output node $\boldsymbol{y}$.

3. Application

We next describe the utilization of the neural network classifier for the local combustion regime identification in a laminar edge flame. The edge flame is a co-flow flame whose inner jet is a mixture of methane and nitrogen with a mass ratio of CH_4:N_2=0.65:0.35, and whose outer jet is air. The computational domain is 2D planar, the fuel inflow width is 2 mm while the splitter plate thickness is 0.38 mm, the domain width is 5.5 cm while the domain length is 12 cm. Both the fuel and oxidizer streams are fed at ambient temperature and atmospheric pressure, at the velocity of 0.35 m/s. The far field is modeled by imposing the total pressure of 1 atm and zero velocity gradient. The splitter plate is modelled as a no-slip adiabatic wall. The computational mesh is structured and with squared cell down to 100 micron in both axial and transverse directions in the injection region. The fuel injector is discretized with 30 cells in the transverse direction, the splitter plate thickness with 6 cells, while the grid mildly coarsens getting further away from the injector, for a total number of 85000 cells. The configuration is sketched in Fig. 2. The computation was performed relying on the pressure-based solver laminarSMOKE, developed by Cuoci et al. [42, 43] within the openFoam framework. In the laminarSMOKE solver, thermochemical properties as well as the chemical source terms are computed by means of the OpenSMOKE++ libraries [44]. The kinetic scheme is the 82-species, 1698-reactions, C1-C3 high-temperature mechanism developed by the CRECK modeling group [45].

The binary classifier is trained with a database $D = \{\boldsymbol{x}_1, ..., \boldsymbol{x}_{N_{samples}}\}$ of labeled thermochemical states $\boldsymbol{x}_i = \{T, Y_j\}$, where T is temperature, Y_j is the mass frac-

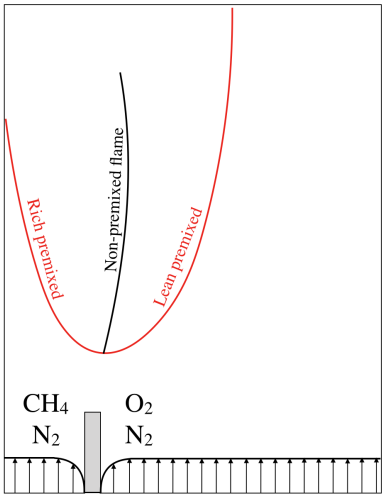

Figure 2.: Sketch of the edge flame configuration.

tion of species j, so that $\boldsymbol{x}_i \in \mathbb{R}^N$. The states $\boldsymbol{x}_i$ are computed as solutions of both steady 1D laminar premixed flames, with different fresh mixture equivalence ratio, and counterflow problems, with different strain rates. The choice of the parameters of the training problems, i.e., boundaries and strain rate, is made based on the edge flame geometry and inflow conditions. Specifically, the 1D premixed flames solutions are obtained for CH_4/Air mixtures at ambient temperature and pressure, having equivalence ratios ranging from 0.5 to 3. The corresponding mixture fraction values are $z \approx 0.05 \div 0.31$, with the stoichiometric mixture fraction placed at $z_{st} \approx 0.1$. The counterflow flames have the two boundaries corresponding to the inflow conditions of the coflow flame, and strain rates ranging from 0.1 to 125 s^{-1}, corresponding to stoichiometric scalar dissipation rates χ_{st} of 10^{-2} to 25 s^{-1}. The computations are performed with openSMOKE++ [44], adopting the same kinetic scheme employed in the coflow flame simulation. The total number of thermochemical states is $N_{samples}$=15000, evenly shared by the two problems and computed with the same prescribed accuracy in the solvers. Figure 3 shows the projection in the (z-T) space of the thermochemical states of the two problems. Each of the premixed solutions, in red, is characterized by a specific value of mixture fraction z; the solutions span a mixture fraction range in between the flammability limits of the mixture. The counterflow solutions, black lines, span the whole z-space.

The classifier is trained on this data set. As a common practice, a k-fold cross-validation is performed, in which the data are randomly partitioned into k equal-sized subsets, with k=100 in this work. Of the k subsets, a single subset is retained as validation data for testing the classifier, and the remaining k-1 are used as training data. The process is performed k times, with each of the k subsets used only once as the validation set. The k results are then averaged to produce a single estimation of accuracy. The 100-fold cross-validation yielded a 99.9% average accuracy score. This result shows that the two classes are well segregated in the composition space and that the classifier is able to discriminate them. Moreover, the k-fold cross-validation ruled out the possibility of overfitting. Based on this result, we did not increase the number of samples.

The k-fold cross-validation is repeated employing samples from the reduced composition space $\bar{\mathbb{S}}$, such that $\bar{\boldsymbol{x}}_i = \{T, N_2, CO_2, H_2O, CO, H_2, CH_4, O_2\} \in \mathbb{R}^8$, yielding the

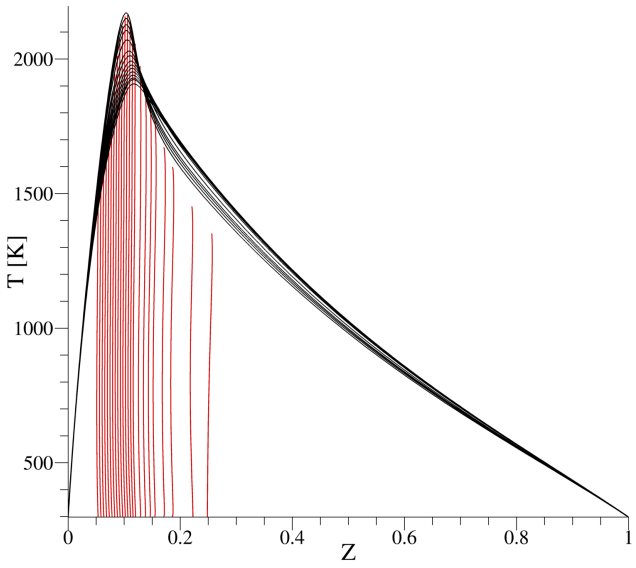

Figure 3.: Projection in the (z-T) space of the thermochemical states originating from 1D premixed (red) and counterflow (black) solutions.

same average accuracy result. This is a clear indication that a low-rank structure exists for both classes, and the embeddings are well separated in composition space. From now on, the data set restricted to the subspace $\bar{\mathbb{S}}$ will be employed, to be compatible with availability of experimental measures, as done in [13].

Moreover, the sensitivity of the network structure and accuracy to the range of χ_{st} in the training dataset is evaluated, showing that the nonpremixed embedding is successfully learnt even with a narrower range of χ_{st}, namely 10 to 100 s^{-1}.

The complete data set in $\bar{\mathbb{S}}$ is finally used to train the classifier, with a 15 % split of the data points for the validation. The Neural Network architecture, whose properties are summarized in Table 1 and whose layers structure is depicted in Fig. 4, has been chosen among a family of alternative configurations. Such configurations differ in the number of hidden layers (2, 4, 8), the number of training epochs (1, 3, 10, 30, 100, 300, 1000) and the presence/absence of an alpha-dropout layer, whose function is described below. These 42 configurations are trained on small datasets (500 samples) and the information gathered during these "experiments" are used to predict how well the configurations would perform on the full dataset. The most promising configurations in which the mean cross-entropy loss is smaller than 0.01 are then trained on a larger dataset (1500 samples), and then on the full training dataset. The best architecture resulted as the one with 2 hidden layers, 300 epochs and Alpha-dropout layer. The architecture is detailed as follows: the network is fully connected and the 2 hidden layers have 50 neurons each. The activation functions are the Scaled Exponential Linear Unit (SELU) in both layers:

$$\mathrm{selu}(x) = \lambda \begin{cases} x & \text{if } x > 0 \\ \alpha e^x - \alpha & \text{if } x \leqslant 0 \end{cases} \tag{4}$$

where x denotes the input, $\alpha = 1.6733$ and $\lambda = 1.0507$. Such functions naturally self-normalize the network, meaning that the network preserves the zero-mean and

Network depth	2
Activation Functions	SELU
Dropout Layer probability	0.01
Loss function	cross-entropy
Optimization method	ADAM
Mean cross-entropy	0.0018
Mean accuracy	0.99989

Table 1.: Neural network properties and performance

unitary-variance nature of the inputs [46]. For this reason, the data set is logarithmically rescaled and standardized to have zero mean and unitary variance before being employed for training. The SELU functions have the advantage to converge faster than the classic activation functions towards the optimum parameters, i.e. weights and biases, and, more importantly, both the vanishing and exploding gradient problems have been demonstrated to be impossible [46]. The first hidden layer has an additional alpha-dropout layer. Dropout layers prevent overfitting by randomly turning off some of the neurons on each iteration of the training, together with all its input and output connections, so that they are not affected by the gradient updates. Alpha-dropout is an enhanced version of dropout, typically employed in conjunction with SELU functions, in which the neurons are not set to 0, but to the negative saturation value of the SELU, preserving the original mean and variance of the inputs and ensuring the self-normalizing property even after dropout. The probability of dropout is set to 1%. The output layer has a softmax activation to produce two decimal numbers between 0 and 1 which sum to 1:

$$\sigma(x)_i = \frac{e^{x_i}}{\sum_{j=1}^{2} e^{x_j}} \qquad i = 1, 2. \tag{5}$$

The employed loss function is the cross-entropy loss, the batch size is 16 and the stochastic optimization algorithm is the adaptive moment estimation (ADAM) [47].

The trained classifier is then fed with states $\bar{\boldsymbol{x}}_i^*$ originating from the edge flame. For each state, the classifier returns a probability of belonging to either the premixed or nonpremixed regime. Note that the two probabilities sum to 1.

4. Discussion

Figure 5a shows the values of $P(\text{class}=\textit{premixed} \,|\, \boldsymbol{x})$ in the edge flame. The red regions are the points in which this probability takes values of 1, or close to 1, hence they are classified as belonging to the premixed regime. The white regions contain the points in which it takes values of 0, or close to 0, hence they are classified as nonpremixed. The rich and lean premixed branches of the flame are clearly distinguishable, as well as the trailing nonpremixed flame. The transition layers between the two regimes, coloured in blue, i.e., where the posterior probability is uninformative, being close to 0.5, are remarkably thin. In other words, there are only a small number of points at which the classifier struggles to make a decision. Figure 5b shows the temperature field of the flame, with mixture fraction iso-contour lines, with the hard classification boundary $P(\text{class}=\textit{premixed} \,|\, \boldsymbol{x})=0.5$ superposed, further confirming the validity of

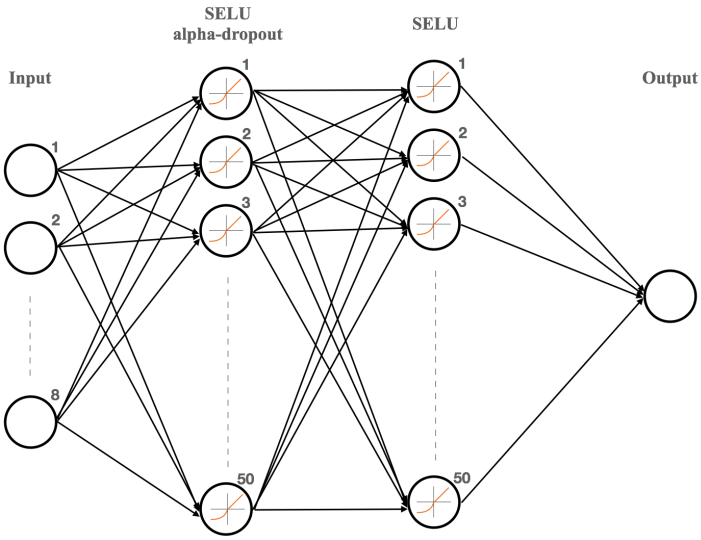

Figure 4.: Sketch of a the employed neural network architecture.

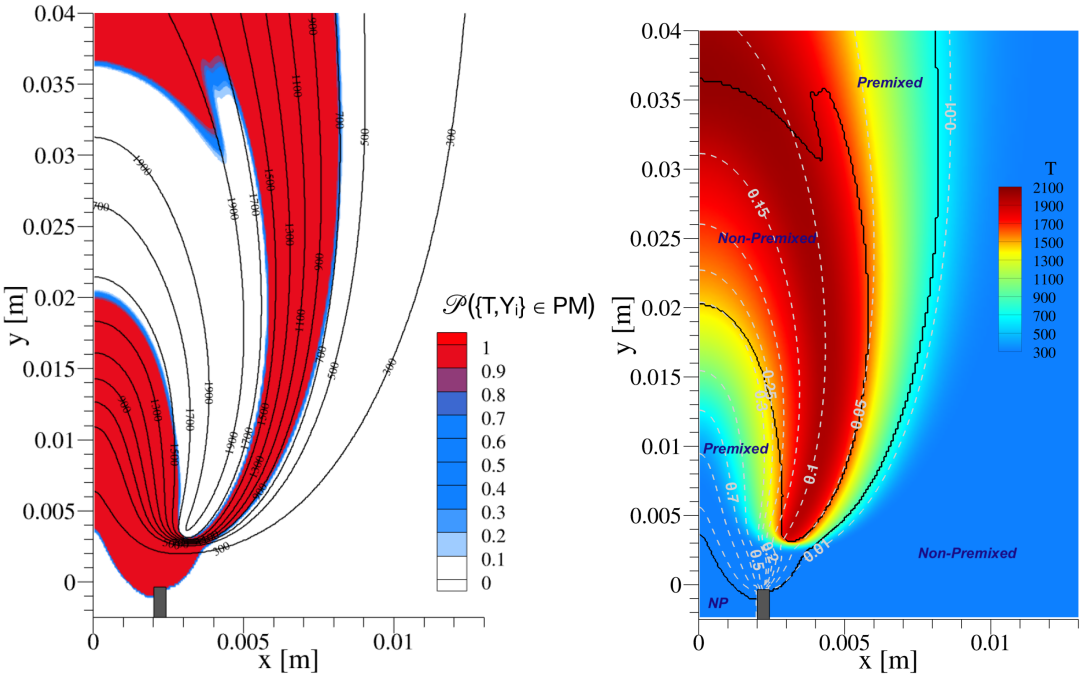

(a) (b)

Figure 5.: (a) $P(\text{class}{=}\textit{premixed}\,|\,\boldsymbol{x})$ in the edge flame field, with temperature iso-contour lines superposed; (b): hard classification boundary $P(\text{class}{=}\textit{premixed}\,|\,\boldsymbol{x}){=}0.5$ -black line- in the edge flame temperature field, with mixture fraction iso-contour lines in gray. Abbreviations are used in the figures: PM (premixed) and NP (nonpremixed).

the transition layer definition.

Figures 6a and 6b show the scatters of the data points in the edge flame solution mapped on the mixture fraction space against temperature and progress variable C, respectively, coloured by $P(\text{class}{=}\textit{premixed}\,|\,\boldsymbol{x})$ such that the premixed states are in

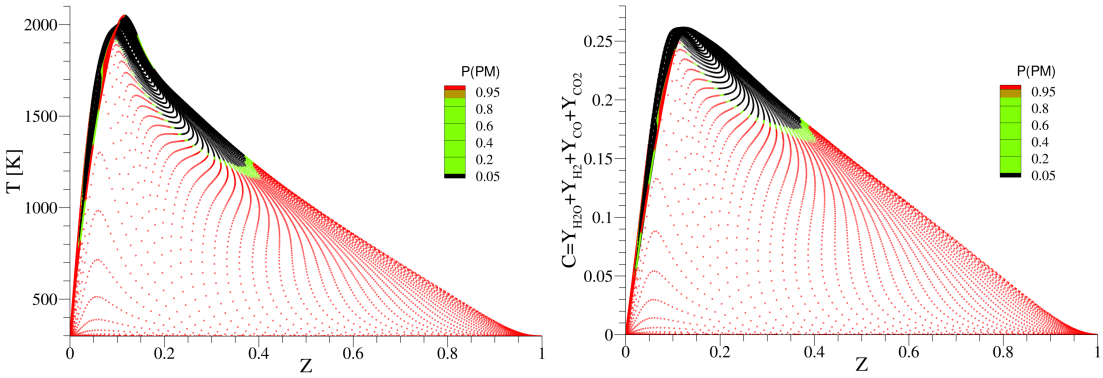

(a) (b)

Figure 6.: Scatters of the edge flame field temperature T (a) and progress variable C (b) against mixture fraction z, colored by $P(\text{class}{=}\textit{premixed}\,|\,\boldsymbol{x})$.

red and the nonpremixed are in black. The high-temperature black points belong to the trailing diffusion flame. The premixed regime is identified throughout the whole z-space, at both low and high temperatures. Note that the transition from the premixed to the nonpremixed classification in the high-temperature states does not appear to be identifiable solely based on the values of C and z, or their combination. This is an indication that the two embeddings have more features than what C and z are able to describe. Such features are learned by the classifier, which is able to distinguish among close or overlapping states in the z-T/z-C planes. Such overlapping, also visible in the training set of Fig.3, is "apparent" because of the projection onto a lower-dimensional space, while the embeddings in the composition space $\bar{S}$ are well separated.

The broad range of the scatters in z for the premixed regime is expected, due to the states belonging to the lean and rich branches of the edge flame. However, the extreme z conditions beyond the typical lean and rich flammability limits are identified as the premixed regime as well. These states belong to the rich/lean pre-heat zones of the edge flame which are, while outside the flammability range, back-supported by diffusion of heat and radicals from flammable premixed regions. The dynamics characterizing these zones would be described by the temporal evolution of a purely diffusive problem in the mixture fraction space in which the high-temperature boundary is the richest/leanest flammable solution and the z=1/z=0 boundary is the cold fuel/oxidizer stream. The classifier associates these points to the premixed class with a high probability since their composition is close to the premixed embedding. If necessary, however, out-of-flammability states can be specifically identified *a priori* based solely on composition, without the need for an additional class, and thus was excluded from the present classification task.

As shown in Fig. 5, the classifier detects a premixed tail behind the trailing non-premixed flame. This tail contains states in or close to the chemical equilibrium which are not represented by the 1D counterflow problems with non-zero strain rate. On the contrary, they are similar to the hot (burnt) boundaries of the 1D premixed flames. A zero-strain nonpremixed flame would share the same thermochemical states with the burnt conditions of the 1D premixed flames inside the flammability limits, creating a class superposition and hence lead to an ambiguous classification. Being the equilibrium composition identifiable without ambiguity, we decided not to define a specific class for such occurrence.

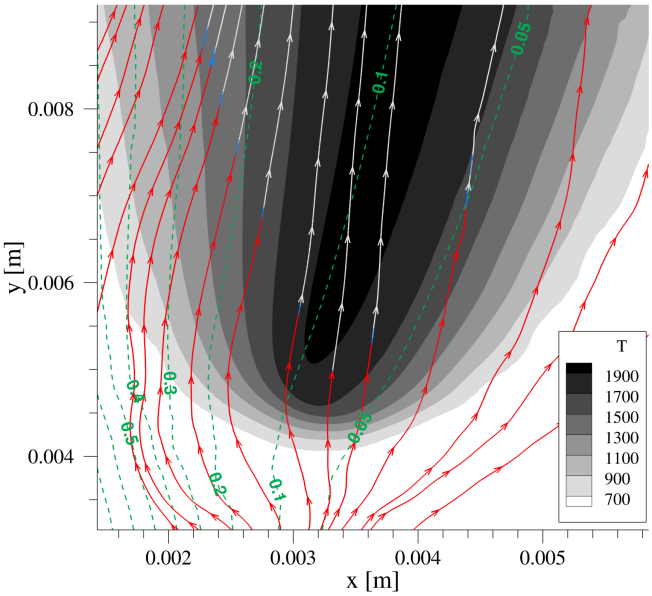

Figure 7.: Up-close on the edge of the flame. Temperature is in grayscale, mixture fraction iso-contour lines in green, streamlines are coloured by $P(class = premixed \,|\, \boldsymbol{x})$ using the colour scale of Fig.5a.

Figure 7 shows a zoomed-in view of the flame edge region. The streamlines are coloured by the classifier probability $P(\text{class}{=}premixed \,|\, \boldsymbol{x})$. A correlation can be noticed between the nonpremixed regime detection (white streamlines) and the alignment between temperature and mixture fraction iso-contour lines.

A comparison with the normalized flame index [10], computed with the gradients available in the edge flame simulation, is shown in Fig. 8. A positive flame index, depicted in red, indicates the premixed regime, while a negative flame index, in blue, indicates the nonpremixed flame. There is good agreement on the lean premixed branch and an acceptable agreement on the trailing diffusion flame. The nonpremixed/premixed transition in the rich side is not captured by the classifier as well as the flame index does, for the reasons discussed above. The immediate upstream of the flame edge, where the cold streams are mixing, is identified as premixed by the classifier, while the flame index indicates a purely nonpremixed regime. In this region, even though the gradients of fuel and oxidizer are definitely opposed, the local thermochemical states have the features of the cold boundaries of the 1D premixed flames. The inlet streams, being either pure fuel or oxidizer, are classified as nonpremixed, for their similarity to the 1D counter-flow flame boundaries. Also in this case, the inert mixing of reactants upstream of the flame front can be identified based on mixture temperature, without resorting to a classifier. Figure 9 shows the classification results with properly excluding the out-of-flammability and inert mixing regions. This confirms the qualitative agreement already observed in Fig. 8, with the major discrepancies appearing at the rich boundary of the trailing diffusion flame. Note, however, that the flame index itself has inherent uncertainties in defining the transition to the diffusion flame (shown in white, where the index is close to zero).

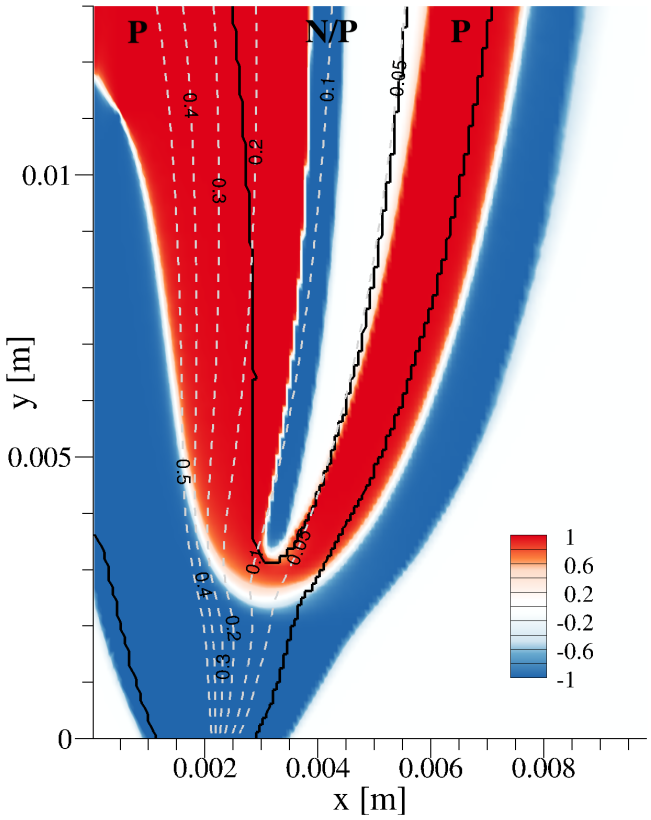

Figure 8.: Comparison between normalized flame index (colored contours) and the current classification $P(\text{class}=\textit{premixed}\,|\,\boldsymbol{x})$=0.5 (black line). Mixture fraction isocontours are overlaid as dashed lines.

5. Conclusions

We proposed a general strategy for combustion regime identification that relies on supervised machine learning. A classification algorithm is instructed to discriminate between premixed and nonpremixed modes by learning from solutions of prototypical problems. The classification deals with thermochemical states only, i.e., local information, without the need for spatial information such as gradients, and accounts for major species only, in line with the experimental availability of data. We assessed the capabilities of the classifier by training it with 1D laminar steady premixed and counterflow solutions and then examining a 2D laminar edge flame, which is an example of multi-regime reacting flow. The classifier proved to be effective in labelling the thermochemical states of the edge flame, given the training data set, which was purposely limited to steady and burning solutions. The rich/lean premixed branches and the trailing diffusion flame are identified with an accuracy comparable to that of the flame index, which relies on gradients of fuel and oxidizer.

Ongoing work will further explore the possibility of adding more classes to characterize other regimes, such as auto-ignition and extinction, employing additional prototypical problems to train the classifier, such as homogeneous reactors and unsteady flamelets. The addition of more classes will help assess the generality of this approach, which is based on the conjecture that a segregation in the composition space of the thermochemical states originating from different combustion regimes exists. This con-

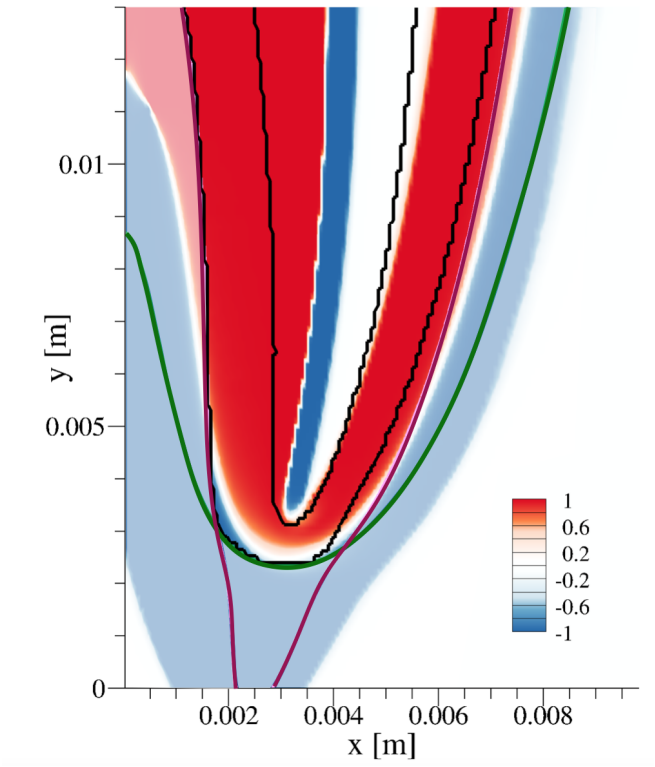

Figure 9.: Comparison between normalized flame index (colored contours) and the current classification (black line), with the exclusion of out-of-flammability regions (outside the magenta lines) and inert mixing (below the green line)

jecture was proved satisfyingly right in this paper in the case of premixed/nonpremixed embeddings. Ongoing work will shed light on the segregation between other combustion regimes. We will also test the classifier with uncertain data, to mimic experimental data, and within a turbulent flame context, outlining further the utility of the present construction for robustly identifying combustion modes and enable a fast closure model selection in the LES context.

Disclosure statement

The authors declare that they have no conflict of interest.

Funding

This work was supported by KAUST OSR-2019-CCF-1975-35 Subaward Agreement.

References

[1] A R Masri. Partial premixing and stratification in turbulent flames. *Proceedings of the Combustion Institute*, 35(2):1115–1136, 2015.

[2] C. J. Lawn. Lifted flames on fuel jets in co-flowing air. *Progress in Energy and Combustion Science*, 35(1):1–30, 2009.
[3] J. Buckmaster. Edge-flames. *Progress in Energy and Combustion Science*, 28(5):435–475, 2002.
[4] Kevin M. Lyons. Toward an understanding of the stabilization mechanisms of lifted turbulent jet flames: Experiments. *Progress in Energy and Combustion Science*, 33(2):211–231, 2007.
[5] J. A. van Oijen and L. P.H. de Goey. A numerical study of confined triple flames using a flamelet-generated manifold. *Combustion Theory and Modelling*, 8(1):141–163, 2004.
[6] Pascale Domingo, Luc Vervisch, and Ken Bray. Partially premixed flamelets in LES of nonpremixed turbulent combustion. *Combustion Theory and Modelling*, 6(4):529–551, 2002.
[7] Pascale Domingo, Luc Vervisch, and Julien Réveillon. Dns analysis of partially premixed combustion in spray and gaseous turbulent flame-bases stabilized in hot air. *Combustion and Flame*, 140(3):172 – 195, 2005.
[8] E Knudsen and H Pitsch. A general flamelet transformation useful for distinguishing between premixed and non-premixed modes of combustion. *Combustion and Flame*, 156(3):678–696, 2009.
[9] E. Knudsen and H. Pitsch. Capabilities and limitations of multi-regime flamelet combustion models. *Combustion and Flame*, 159(1):242–264, 2012.
[10] H Yamashita, M Shimada, and T Takeno. A numerical study on flame stability at the transition point of jet diffusion flames. *Proceedings of the Combustion Institute*, pages 27–34, 1996.
[11] B. Fiorina, O. Gicquel, L. Vervisch, S. Carpentier, and N. Darabiha. Approximating the chemical structure of partially premixed and diffusion counterflow flames using FPI flamelet tabulation. *Combustion and Flame*, 140(3):147–160, 2005.
[12] David A Rosenberg, Patton M Allison, and James F Driscoll. Flame index and its statistical properties measured to understand partially premixed turbulent combustion. *Combustion and Flame*, 162(7):2808–2822, 2015.
[13] Sandra Hartl, Dirk Geyer, Andreas Dreizler, Gaetano Magnotti, Robert S Barlow, and Christian Hasse. Regime identification from Raman / Rayleigh line measurements in partially premixed flames. *Combustion and Flame*, 189:126–141, 2018.
[14] U.Maas and S.B.Pope. Simplifying chemical kinetics: Intrinsic low dimensional manifolds in composition space. *Combustion and Flame*, 88:239–264, 1992.
[15] S.H. Lam. Using CSP to Understand Complex Chemical Kinetics. *Combustion Science and Technology*, 89:375–404, 1993.
[16] Sharath S Girimaji. Composition-Space Behavior of Diffusion-Reaction Systems. *Theoretical and Computational Fluid Dynamics*, 17(3):171–188, 2004.
[17] Olivier Gicquel, Nasser Darabiha, and Dominique Thévenin. Liminar premixed hydrogen/air counterflow flame simulations using flame prolongation of ildm with differential diffusion. *Proceedings of the Combustion Institute*, 28(2):1901 – 1908, 2000.
[18] H. Bongers, J.A. Van Oijen, and L.P.H. De Goey. Intrinsic low-dimensional manifold method extended with diffusion. *Proceedings of the Combustion Institute*, 29(1):1371 – 1378, 2002.
[19] Dimitris A. Goussis, Mauro Valorani, Francesco Creta, and Habib N. Najm. Reactive and reactive-diffusive time scales in stiff reaction-diffusion systems. *Progress in Computational Fluid Dynamics, An International Journal*, 5(6):316, 2005.
[20] Habib N. Najm, Mauro Valorani, Dimitris A. Goussis, and Jens Prager. Analysis of methane–air edge flame structure. *Combustion Theory and Modelling*, 14(2):257–294, 2010.
[21] J. D. Mengers and J. M. Powers. One-dimensional slow invariant manifolds for fully coupled reaction and micro-scale diffusion. *SIAM Journal on Applied Dynamical Systems*, 12(2):560–595, 2013.
[22] V. Bykov and U. Maas. The extension of the ildm concept to reaction–diffusion manifolds.

Combustion Theory and Modelling, 11(6):839–862, 2007.

[23] J. A. Van Oijen, F. A. Lammers, and L. P.H. De Goey. Modeling of complex premixed burner systems by using flamelet-generated manifolds. *Combustion and Flame*, 127(3):2124–2134, 2001.

[24] Phuc Danh Nguyen, Luc Vervisch, Vallinayagam Subramanian, and Pascale Domingo. Multidimensional flamelet-generated manifolds for partially premixed combustion. *Combustion and Flame*, 157(1):43–61, 2010.

[25] James C. Sutherland and Alessandro Parente. Combustion modeling using principal component analysis. *Proceedings of the Combustion Institute*, 32 I(1):1563–1570, 2009.

[26] Tarek Echekki and Hessam Mirgolbabaei. Principal component transport in turbulent combustion: A posteriori analysis. *Combustion and Flame*, 162(5):1919–1933, 2015.

[27] Hao Wu and Matthias Ihme. Compliance of combustion models for turbulent reacting flow simulations. *Fuel*, 186:853 – 863, 2016.

[28] Thorsten Zirwes, Feichi Zhang, Peter Habisreuther, Maximilian Hansinger, Henning Bockhorn, Michael Pfitzner, and Dimosthenis Trimis. Identification of Flame Regimes in Partially Premixed Combustion from a Quasi-DNS Datasets. *Flow, Turbulence and Combustion*, 2020.

[29] Steven L. Brunton and J. Nathan Kutz. *Data-Driven Science and Engineering: Machine Learning, Dynamical Systems, and Control*. Cambridge University Press, 2019.

[30] K. P. Grogan and M. Ihme. Identification of governing physical processes of irregular combustion through machine learning. *Shock Waves*, 28(5):941–954, 2018.

[31] Giuseppe D'Alessio, Alessandro Parente, Alessandro Stagni, and Alberto Cuoci. Adaptive chemistry via pre-partitioning of composition space and mechanism reduction. *Combustion and Flame*, 211:68–82, 2020.

[32] Ian Goodfellow, Yoshua Bengio, and Aaron Courville. *Deep Learning*. The MIT Press, 2016.

[33] Eric B. Baum and Frank Wilczek. Supervised learning of probability distributions by neural networks. In D. Z. Anderson, editor, *Neural Information Processing Systems*, pages 52–61. American Institute of Physics, 1988.

[34] Robert P. W. Duin and David M. J. Tax. Classifier conditional posterior probabilities. In Adnan Amin, Dov Dori, Pavel Pudil, and Herbert Freeman, editors, *Advances in Pattern Recognition*, pages 611–619, Berlin, Heidelberg, 1998. Springer Berlin Heidelberg.

[35] Michael D. Richard and Richard P. Lippmann. Neural network classifiers estimate bayesian a posteriori probabilities. *Neural Computation*, 3(4):461–483, 1991. PMID: 31167331.

[36] Richard P. Lippmann. Neural networks, bayesian a posteriori probabilities, and pattern classification. In Vladimir Cherkassky, Jerome H. Friedman, and Harry Wechsler, editors, *From Statistics to Neural Networks*, pages 83–104, Berlin, Heidelberg, 1994. Springer Berlin Heidelberg.

[37] Raúl Rojas. A short proof of the posterior probability property of classifier neural networks. *Neural Comput.*, 8(1):41–43, January 1996.

[38] Herbert Gish. A probabilistic approach to the understanding and training of neural network classifiers. *International Conference on Acoustics, Speech, and Signal Processing*, pages 1361–1364 vol.3, 1990.

[39] E. A. Wan. Neural network classification: a bayesian interpretation. *IEEE Transactions on Neural Networks*, 1(4):303–305, 1990.

[40] D. W. Ruck, S. K. Rogers, M. Kabrisky, M. E. Oxley, and B. W. Suter. The multilayer perceptron as an approximation to a bayes optimal discriminant function. *IEEE Transactions on Neural Networks*, 1(4):296–298, 1990.

[41] Ming S. Hung. Estimating posterior probabilities in classication problems with neural networks. 1996.

[42] Alberto Cuoci, Alessio Frassoldati, Tiziano Faravelli, and Eliseo Ranzi. A computational tool for the detailed kinetic modeling of laminar flames: Application to c2h4/ch4 coflow flames. *Combustion and Flame*, 160(5):870 – 886, 2013.

[43] Alberto Cuoci, Alessio Frassoldati, Tiziano Faravelli, and Eliseo Ranzi. Numerical modeling of laminar flames with detailed kinetics based on the operator-splitting method. *Energy and Fuels*, 27(12):7730–7753, 2013.

[44] A. Cuoci, A. Frassoldati, T. Faravelli, and E. Ranzi. Opensmoke++: An object-oriented framework for the numerical modeling of reactive systems with detailed kinetic mechanisms. *Computer Physics Communications*, 192:237 – 264, 2015.

[45] E. Ranzi, A. Frassoldati, R. Grana, A. Cuoci, T. Faravelli, A.P. Kelley, and C.K. Law. Hierarchical and comparative kinetic modeling of laminar flame speeds of hydrocarbon and oxygenated fuels. *Progress in Energy and Combustion Science*, 38(4):468 – 501, 2012.

[46] Günter Klambauer, Thomas Unterthiner, Andreas Mayr, and Sepp Hochreiter. Self-normalizing neural networks. In *Proceedings of the 31st International Conference on Neural Information Processing Systems*, NIPS'17, page 972–981, Red Hook, NY, USA, 2017. Curran Associates Inc.

[47] Diederik P. Kingma and Jimmy Ba. Adam: A method for stochastic optimization, 2014. cite arxiv:1412.6980Comment: Published as a conference paper at the 3rd International Conference for Learning Representations, San Diego, 2015.